

OPEN ACCESS

Contrast Matched SANS for Observing SEI and Pore Clogging in Silicon-Graphite Anodes

To cite this article: Neelima Paul *et al* 2019 *J. Electrochem. Soc.* **166** A1051

View the [article online](#) for updates and enhancements.



Contrast Matched SANS for Observing SEI and Pore Clogging in Silicon-Graphite Anodes

Neelima Paul,^{1,z} Morten Wetjen,^{1,z} Sebastian Busch,³ Hubert Gasteiger,^{2,*} and Ralph Gilles¹

¹Heinz Maier-Leibnitz Zentrum, Technische Universität München, 85748 Garching, Germany

²Chair of Technical Electrochemistry, Department of Chemistry and Catalysis Research Center, Technische Universität München, 85748 Garching, Germany

³German Engineering Materials Science Centre (GEMS) at Heinz Maier-Leibnitz Zentrum (MLZ), Helmholtz-Zentrum Geesthacht GmbH, 85748 Garching bei München, Germany

Silicon-graphite (SiG) electrodes are attractive candidates as anodes for Li-ion batteries due to their high theoretical specific capacity. However, repeated lithiation/delithiation during charge/discharge cycling causes significant morphological changes of the silicon particles. This results in the formation of highly porous silicon structures and severe side reactions at the silicon/electrolyte interface. To quantify these morphological changes, small-angle neutron scattering (SANS) was applied with selective contrast matching of Si nanoparticles (200 nm diameter) and the surrounding electrolyte decomposition products. Using electrolytes consisting of 1.5 M LiPF₆ dissolved in either deuterated or protonated ethylene carbonate (EC) resulted in solid-electrolyte-interphase (SEI) compounds with scattering length densities either matching or mismatching that of the Si nanoparticles. SiG anodes with 35 wt% silicon nanoparticles were aged for 10 and 20 charge/discharge cycles against capacitively oversized LiFePO₄ cathodes. Afterwards, the morphological changes and size distribution of the SEI compounds were evaluated by means of ex-situ SANS measurements of the SiG electrodes in their fully discharged state. Transmission electron microscopy (TEM) images of the pristine and cycled silicon nanoparticles complement the interpretation of the SANS analysis.

© The Author(s) 2019. Published by ECS. This is an open access article distributed under the terms of the Creative Commons Attribution 4.0 License (CC BY, <http://creativecommons.org/licenses/by/4.0/>), which permits unrestricted reuse of the work in any medium, provided the original work is properly cited. [DOI: 10.1149/2.0781906jes]



Manuscript submitted December 10, 2018; revised manuscript received March 11, 2019. Published April 2, 2019.

For Li-ion batteries, silicon is an attractive alternative to graphite due to its high theoretical specific capacity of 3579 mAh g⁻¹.¹ However, Si-based anodes undergo severe morphological changes upon repeated lithiation/delithiation, resulting in a high irreversible capacity and poor cycling stability. Previous studies using electron microscopy provided valuable insights into the degradation of such electrodes.²⁻⁵ Recently, Wetjen et al. reported that within few cycles, initially compact Si particles start to transform into nanoporous structures with a high surface area. In less than 20 cycles, this can result in a considerable expansion of the Si particles also in their delithiated state.⁶ By means of STEM-EDS and SEM analysis, it was shown that these pores were filled with fluorine- and oxygen-containing SEI products which also cover the fragmented Si nanostructures. To quantify the underlying morphological changes upon charge/discharge cycling, further information such as thickness of the SEI surface layer, size, and volume of pores in such degraded Si particles is required. Moreover, depending on the magnification, electron microscopy is usually restricted to small areas of the electrode coating but does not capture the morphology of the entire electrode.

Small-angle neutron scattering (SANS) is a powerful method for determining statistically averaged lateral morphologies of nanostructures on the order of 1–100 nm. It is representative of the entire sample up to several hundred cubic millimeters and has been often used to study lithiation mechanisms into carbons:⁷⁻¹¹ when imaging electrodes with thicknesses up to several hundred μm, the entire electrode volume for electrode areas up to 20 cm² can be probed by SANS. The neutrons interact with the different nuclei in the sample at different strengths, called the scattering length density (SLD) which is a measure of scattering power. The difference between the SLDs of the nanosized inhomogeneity and the matrix within which it is dispersed is known as the scattering contrast: If the SLDs are equal, the inhomogeneity is invisible to the neutrons (there is no contrast), whereas the inhomogeneities can be distinguished well if the SLDs are not matched, providing a contrast between nanosized inhomogeneity and the surrounding matrix. Since the SLDs are isotope-dependent, it is possible to highlight or mask different parts of the sample by exchanging for example hydrogen for deuterium. In the field of nanoporous carbons, contrast

matched SANS has already been used to investigate microstructures of pores and their accessibility to organic solvents.^{12,13,14} More recently, in-situ contrast matched SANS was used to monitor SEI formation on carbon surfaces in half-cells.¹⁵ SANS studies in the field of Li-ion batteries are generally focused on single-element carbon system. To our knowledge, there is no SANS manuscript on complicated two-element SiG electrode system, which is a very promising candidate to be an extremely high capacity anode (in comparison to conventionally used graphite) for Li-ion batteries.

Here, we expand this concept to characterize the morphological changes of silicon nanoparticles in silicon-graphite (SiG) electrodes for Li-ion batteries. Conducting SANS on harvested SiG electrode after repeated charge/discharge cycling in a coin cell, we obtained relevant morphological details from the entire SiG electrode area (1.5 cm²), quantifying the average SEI thickness and the pore volume of the degraded Si particles. To accomplish this, we used the contrast matching technique by cycling the SiG electrodes in different electrolytes, consisting of 1.5 M LiPF₆ dissolved in either deuterated or protonated ethylene carbonate (EC), in order to vary the SLDs of the SEI products and their differences to the SLD of the Si particles. Previous contrast-variation SANS studies typically achieve contrast matching by simply immersing the sample in solvent containing different ratios of protonated and deuterated solvents.

Materials and Methods

Electrode preparation.—SiG electrodes with a mass loading of ~1.4 mg cm⁻² and a theoretical areal capacity of ~2.0 mAh cm⁻² (assuming 3579 mAh g⁻¹_{Si} and 372 mAh g⁻¹_C) were prepared by casting an aqueous ink onto 20 μm thick Cu-foil. The resulting electrode composition consisted of 35 wt% Si nanoparticles (~200 nm diameter, Wacker AG, Germany), 45 wt% graphite (~20 μm diameter), 10 wt% carbon fibers and 10 wt% lithium poly(acrylate) (LiPAA) binder (for details see Ref. 6).

Cell assembly.—Coin cells were prepared by sandwiching two glass-fiber separators between a SiG anode (14 mm), and a capacitively oversized LiFePO₄ (LFP) cathode (3.5 mAh cm⁻², Custom Cells, Germany; see Ref. 16). Two different electrolytes were used, consisting of 1.5 M LiPF₆ dissolved in either protonated ethylene carbonate

*Electrochemical Society Fellow.

^zE-mail: Neelima.Paul@frm2.tum.de

(EC, BASF, Germany) or deuterated ethylene carbonate (EC-d4, 99 atom% D enrichment, 99.2% chemical purity, EQ Laboratories GmbH, Germany). After 10 and 20 charge/discharge cycles, the SiG electrodes were extracted from the cells in their fully discharged state and stored in a protective pouch-bag casing for ex-situ SANS measurements. The electrolyte was not transferred with the electrodes and thus the electrodes were in a “matrix” of inert gas.

Cycling protocol.—Electrochemical aging of the SiG electrodes was conducted using a delithiation-limited galvanostatic procedure that reduces the extent of side reactions at the silicon/electrolyte interface.⁶ As the here investigated electrolytes do not contain any additives, e.g., fluoroethylene carbonate (FEC) or vinylene carbonate (VC), this approach offered a reasonable cycling stability. Hence, the SiG electrodes were fully lithiated to 0.01 V vs. Li⁺/Li (3.44 V cell voltage, based on a stable potential of 3.45 V vs. Li⁺/Li for the capacitively oversized LFP counter electrode) and only partially delithiated to 0.65 V vs. Li⁺/Li (2.8 V cell voltage). In a standard FEC-containing electrolyte (1 M LiPF₆ in EC/EMC 3/7 g/g with 5 wt% FEC), these potential limits yield ~71% of the theoretical electrode delithiation capacity over the first 20 cycles at a rate of C/3 (viz., ~1000 of theoretically ~1420 mAh g⁻¹_{el}).⁶ Two formation cycles were conducted at C/10 (~0.2 mA cm⁻²), while subsequent charge/discharge cycling was performed at C/3 (all C-rates are referenced to the above quoted theoretical specific capacity). During the last cycle, the SiG electrode was discharged to ~2.0 V vs. Li⁺/Li (1.45 V cell voltage) using a very low C-rate of C/50 to remove any cyclable lithium from the active materials. The fully discharged SiG electrodes were harvested from the cells, washed with dimethyl carbonate (DMC) in order to remove residual electrolyte, and dried in an inert atmosphere. All electrochemical measurements were performed using a battery cyler (Series 4000, Maccor, USA).

TEM.—The real space morphology of the silicon nanoparticles prior to cycling and after 20 cycles was investigated by high-resolution scanning transmission electron microscopy (STEM), using a FEI Titan Themis (FEI, USA) at 200 kV. Samples were prepared by carefully scratching the previously extracted electrode coatings and pressing a TEM lacey carbon Cu 200 grid (EMS, USA) onto the surface.⁶

SANS.—SANS measurements were performed at the SANS-1 instrument¹⁷ of the Heinz Maier-Leibnitz Zentrum (MLZ). To follow the morphological changes of the silicon particles and the concomitant growth of the SEI as function of cycle number, a combination of sample-detector distances (2–20 m) and neutron wavelengths (6–12 Å) was used, covering a *Q*-range of 0.02 to 3 nm⁻¹. This configuration limits the maximum resolved size to ~100 nm. Consequently, the measurement was not sensitive to scattering from Si particles surrounded by micrometer-sized graphite particles in the porous electrode coating. Instead, only scattering from nanosized inhomogeneities within and around expanded Si nanoparticles was detected. Contrast matching was employed by a careful selection of electrolytes to either match or mismatch the SLD of the Si particles (SLD 2.1 × 10⁻⁶ Å⁻²): either a protonated EC electrolyte (SLD 2.2 × 10⁻⁶ Å⁻²) or a deuterated EC-d4 electrolyte (SLD 5.8 × 10⁻⁶ Å⁻²). Given that gases have an SLD which is nearly 0 (SLD 0.004 × 10⁻⁶ Å⁻²), this made it possible to examine if pores in the expanded Si nanoparticles are empty or clogged with SEI products. The data were reduced with BerSANS¹⁸ using a 1 mm thick H₂O sample in order to render the data in absolute scale. Data analysis was performed with the SasFit software.¹⁹

Results and Discussion

Galvanostatic cycling.—Fig. 1 shows the specific electrode capacity of the SiG anodes during charge/discharge cycling in either ¹H-based EC-only (1.5 M LiPF₆ in EC, blue) or deuterated ²D-based EC-only electrolyte (1.5 M LiPF₆ in EC-d4, green), yielding a first-cycle lithiation capacity at 0.1C between 1250–1400 mAh g⁻¹_{el} (hollow symbols). However, the subsequent delithiation capacity at 0.1C

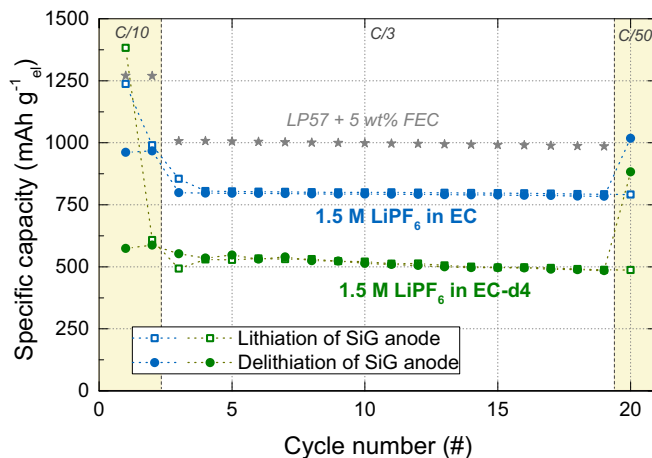


Figure 1. Specific capacity of the SiG anodes in 1.5 M LiPF₆ dissolved in either deuterated EC-d4 (green) or protonated EC (blue) during galvanostatic cycling between 0.01 and 0.65 V vs. Li⁺/Li (3.44 and 2.8 V cell voltage) against a capacitively oversized LiFePO₄ cathode. Two formation cycles were conducted at C/10, followed by cycling at C/3. The last discharge prior to disassembly of the cell was conducted at C/50. The gray asterisks mark the delithiation capacity obtained in a conventional FEC-containing electrolyte (1 M LiPF₆ in EC:EMC (3:7 w:w) + 5 wt% FEC) (see Ref. 6).

is substantially smaller compared to that obtained in a standard FEC-containing electrolyte with the same cutoff potentials (s. gray asterisks in Fig. 1, taken from Ref. 6). In the case of the ¹H-based EC-only electrolyte, this can be explained by an inferior passivation of the silicon/electrolyte interface in the EC-only electrolyte, particularly in the absence of FEC.²⁰ In the case of the deuterated EC-only electrolyte (EC-d4), we believe it is due to the lower chemical purity of the EC-d4 solvent and the associated reductive decomposition of impurities. Nevertheless, by using the delithiation-limited cycling procedure, the cycling stability of the SiG electrodes in both of the EC-only electrolytes is reasonable, with capacity fading rates comparable to what one can obtain with a conventional FEC-containing electrolyte (see gray asterisks in Fig 1). After either 10 or 20 cycles, the SiG electrodes were delithiated at a slow C-rate of C/50 to extract any cyclable lithium. This yielded a delithiation capacity of ~900-1000 mAh g⁻¹, i.e., equal or higher than the delithiation capacity after the 2nd cycle at C/10, indicating that the silicon particles are still accessible, even though the (de-)lithiation at higher C-rates is partially inhibited because of high kinetic overpotentials caused by resistive SEI layers.

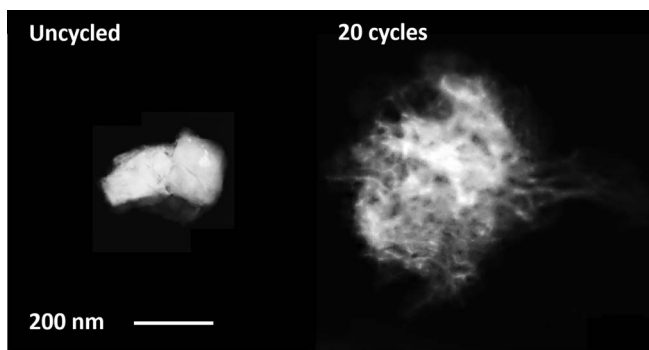


Figure 2. STEM images of individual silicon particles scratched from an SiG anode prior to cycling and after 20 charge/discharge cycle in standard FEC-containing electrolyte. High-angle annular dark field (HAADF) detector, acceleration voltage: 200 kV. Adapted from Wetjen et al.⁶ with permission from The Electrochemical Society (Copyright 2018).

Electrode morphology by TEM.—Fig. 2 shows the STEM images of individual silicon particles scratched from an uncycled electrode (left) and after 20 charge/discharge cycles in standard FEC-containing electrolyte [6] in its delithiated state (right). While the uncycled particles are compact with a mean diameter of ~ 200 nm, after cycling the particles transformed into expanded (mean diameter ~ 500 nm) and highly porous nanostructures. A more detailed investigation of the morphological changes of Si nanoparticles was recently reported by Wetjen et al. [6]. The authors could show with energy dispersive spectroscopy (EDS), at a very local particle level, that there is a distribution of F and O over the entire nanoporous silicon particle. However, it was not possible to distinguish if these F and O elements were merely surrounding the filaments of the Si nanoparticle or also filling up the nanopores within the Si nanoparticle. It was also not clear if the pores were partially or completely filled with these elements.

Contrast-matched SANS.—To quantify the morphological changes of the Si particles and describe the SEI-filled pore volume averaged across the entire electrode coating, SANS measurements were conducted of the SiG electrodes prior to cycling (i.e., pristine) and after 10 and 20 cycles, respectively. A SANS pattern of an aged SiG electrode exhibiting the formation of porous nanostructured silicon particles is expected to show a higher scattering intensity compared to the pristine SiG electrode, owing to an increased scattering contribution from nanostructures in the expanded Si network compared to solid nanopore-free pristine silicon particles. These nanostructures could be pores within the expanded network as well as the SEI layer surrounding the fragmented Si nanoparticles, both well-established consequences of aging. However, as discussed below, without using the contrast-matching SANS technique it is not possible to clarify if the pores in the expanded nanoporous silicon particles are filled with gas or with SEI products.

To address this question, one set of SiG electrodes was cycled in an ^1H -based EC electrolyte whose scattering length density ($2.2 \times 10^{-6} \text{ \AA}^{-2}$) is similar to that of silicon ($2.1 \times 10^{-6} \text{ \AA}^{-2}$), whereas the other set was cycled in an ^2D -based EC-only electrolyte (EC-d4 electrolyte) whose scattering length density ($5.8 \times 10^{-6} \text{ \AA}^{-2}$) is significantly different from that of silicon. As SEI products are formed from the decomposed EC electrolyte (predominantly lithium ethyl dicarbonate),²¹ they are expected to have similar SLDs as the electrolyte solvent. Thus, if pores within the aged and expanded Si nanoparticles were to be filled with SEI products, there would be no SLD contrast with the Si nanoparticles when aging is conducted in a ^1H -based EC-only electrolyte, rendering them as well as the external SEI layers virtually ‘invisible’ to the surrounding Si nanoparticle matrix; on the contrary, when aging is conducted in a ^2D -based EC-only electrolyte, the expected large SLD differences would make the SEI ‘visible’ to the surrounding matrix. On the other hand, if the pores within the aged and expanded silicon particles were not filled with SEI products, the silicon nanopores in the washed electrodes would be filled with gas (SLD of gas ~ 0), in which case the nanopores would remain ‘visible’ to the surrounding matrix, irrespective whether ^1H - or ^2D -based EC-only electrolytes were used. It should be noted that because of the fact that the graphite scattering length density ($6.6 \times 10^{-6} \text{ \AA}^{-2}$) is different from that of ^1H -EC and similar to that of ^2D -EC, pores within the graphite particles would show up only in the SANS spectra of SiG electrodes cycled with the ^1H -based EC-only electrolyte. Nevertheless, the SEI on graphite is not expected to influence these measurements, because the proportional surface area of graphite in the blended SiG electrodes accounts for $\sim 16\%$ of the active materials (assuming BET surface areas of $40 \text{ m}^2 \text{ g}^{-1}$ for silicon and $5 \text{ m}^2 \text{ g}^{-1}$ for graphite) and decreases even further upon lithiation (and expansion) of silicon. As a corollary, the resulting volume fraction of the SEI on graphite is almost negligible in the SANS spectra.

Fig. 3 shows the SANS data of SiG anodes cycled either in (a) ^1H -based EC-only or (b) ^2D -based EC-only electrolyte. The SANS features of the electrodes which were cycled in the ^1H -EC electrolyte

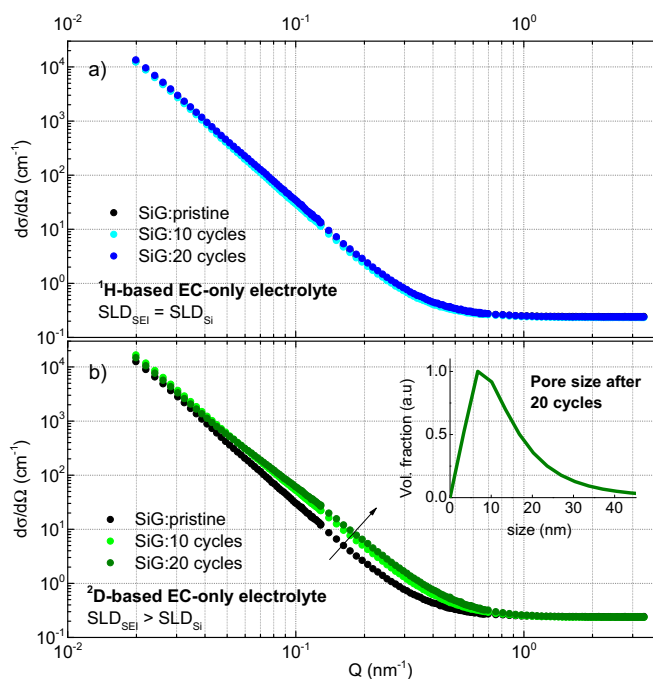
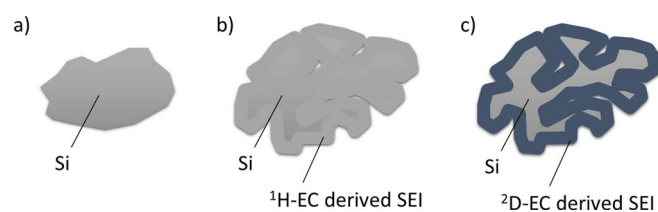


Figure 3. (a) SANS data of SiG electrodes from cells with ^1H -based EC-only electrolyte seem unchanged upon aging over 10 and 20 cycles (here, the SLD of the formed SEI (SLD_{SEI}) is expected to be similar to that of silicon (SLD_{Si})). (b) SANS data of SiG electrodes from cells with ^2D -based EC-only electrolyte show the appearance and growth of nanostructures in the silicon particles upon aging (here, SLD_{SEI} is expected to be larger than that of silicon). The log-normal size distribution obtained from modelling the SANS data is shown in the inset of Fig 3b.

show almost no change with respect to those of the pristine electrodes, which means the pores are completely filled with SEI products having the same SLD as the Si nanoparticles matrix. That is, the pores and formed SEI look the same as the Si nanoparticle to the neutrons and therefore become virtually invisible for SANS. Or, on the other hand, if the pores were not filled with SEI, the very low SLD of gas filling the pores of the washed electrodes would result in a strong scattering contrast. In contrast, a notable increase in the scattering is observed for the electrodes which were cycled in ^2D -based EC-only electrolyte. This indicates that a) the porosity of the Si nanoparticles increases upon cycling and b) that these pores must be largely filled with SEI products. Therefore, they are only visible by SANS when the SLDs of their contents are strikingly different than that of the Si nanoparticles. Our experimental approach and findings are summarized in Scheme 1: a) shows the pristine and dense silicon particle prior to cycling, while b) and c) show the expanded nanoporous silicon particles formed upon cycling, which are filled and covered by SEI products, whereby a



Scheme 1. A sketch explaining the experimental approach and the findings of this study. The SLD contrast between the Si nanoparticles and the porous structure (filled by SEI from decomposed electrolyte), as seen by SANS. The here used SLDs are: $\text{Si} = 2.1 \times 10^{-6} \text{ \AA}^{-2}$, $^1\text{H-EC} = 2.2 \times 10^{-6} \text{ \AA}^{-2}$ (assumed to be closely corresponding to the SEI formed from ^1H -based EC-only electrolyte), and $^2\text{D-EC} = 5.8 \times 10^{-6} \text{ \AA}^{-2}$ (assumed to be closely corresponding to the SEI formed from ^2D -based EC-only electrolyte).

significant SANS contrast is only observed when using ²D-based EC as electrolyte.

The microstructure of the aged SiG electrode (after 20 cycles) was modelled using a hard sphere model and assuming a log-normal size distribution, which is very often used in small-angle scattering evaluations to model size distributions arising from fatigue-stress due to the fact that the derived mean value is close to the average size value.²² Nanostructures with a mean size of 8 nm were estimated, as shown in the inset of Fig. 3b. Due to the fact that the SEI layer around the Si nanoparticles and the SEI within the expanded nano-porous Si nanoparticles have the same SLD, it is not possible to distinguish between them. However, as the pores are expected to have a substantially broader size distribution (as can be deduced from Fig. 2) than the SEI layer thickness, we hypothesize that the broad size distribution ranging up to 30 nm (see inset in Fig. 3b) with a prominent mean size of 8 nm can be attributed to pores within the porous silicon nanoparticle. Moreover, as SEI layer thickness is known to be ca. 18–26 nm without FEC containing electrolytes, this broad size distribution also contains scattering contributions from the SEI layer around Si nanoparticles.²³ Overall, the nanostructures are in good agreement with the porous framework seen in the STEM images of these electrodes in Fig. 2. This confirms that the microscopically observed porous structure which was reported previously is representative for the entire SiG electrode. Methods like EDS could only indicate a distribution of certain elements in the expanded Si particle without clarifying if these elements are just coating the particle edges, surfaces or also filling the pores. Using the contrast variation SANS method and a clever selection of electrolytes for cell cycling, we were not only able to evaluate the mean pore size, pore size distribution in porous Si nanoparticles but we were also able to prove the complete filling of pores with SEI products in a non-destructive manner and without exposure of the electrode to ambient conditions, thereby supporting earlier microscopy measurements with these additional insights.

Conclusions

Contrast matched SANS was applied to SiG electrodes to monitor the morphological changes of Si nanoparticles upon charge/discharge cycling. Our results allow evaluation of the evolving porous nanostructures and confirm their filling with SEI products, showing that the silicon nanoparticles in aged SiG electrodes have a nanoporous microstructure with a prominent mean size of 8 nm and a broad size distribution ranging up to 30 nm (presuming a confidence interval of 90% in the log-normal size distribution). These morphological parameters can be attributed to pores within the porous silicon nanoparticle and to the SEI layer around Si nanoparticles. As a corollary, contrast matched SANS measurements offer a quantitative evaluation of the morphological changes and the concomitant SEI growth in SiG electrodes across their entire thickness and over areas on the order of 2 cm². Our analysis is in good agreement with previous microscopic studies and provides additional quantitative information using the same electrode system (not model electrode) regarding pore size distribution and degree of pore filling.

Acknowledgment

This work was financially supported by the German Federal Ministry of Education and Research (BMBF) and the German Federal Ministry for Economic Affairs and Energy (BMWi) under grant numbers 03XP0081 (ExZellTUM II) and 03ET6045D (LiMo). This work is based upon experiments performed at the SANS-1 instrument operated by TUM and HZG at the Heinz Maier-Leibnitz Zentrum (MLZ), Garching, Germany. Wacker Chemie AG is kindly acknowledged for providing the silicon nanoparticles. This work was supported by the German Research Foundation (DFG) and the Technical University of Munich (TUM) in the framework of the Open Access Publishing Program.

ORCID

Neelima Paul  <https://orcid.org/0000-0002-6906-1683>
 Morten Wetjen  <https://orcid.org/0000-0002-2357-1151>
 Ralph Gilles  <https://orcid.org/0000-0003-2703-4369>

References

1. M. N. Obrovac and V. L. Chevrier, *Chem Rev*, **114**, 11444 (2014).
2. A. L. Michan, G. Divitini, A. J. Pell, M. Leskes, C. Ducati, and C. P. Grey, *Journal of the American Chemical Society*, **138**, 7918 (2016).
3. Y. Oumellal, N. Delpuech, D. Mazouzi, N. Dupré, J. Gaubicher, P. Moreau, P. Soudan, B. Lestriez, and D. Guyomard, *Journal of Materials Chemistry*, **21**, 6201 (2011).
4. M. Wetjen, M. Trunk, L. Werner, R. Gernhauser, B. Markisch, Z. Revay, R. Gilles, and H. A. Gasteiger, *Journal of the Electrochemical Society*, **165**, A2340 (2018).
5. M. T. McDowell, S. W. Lee, W. D. Nix, and Y. Cui, *Adv Mater*, **25**, 4966 (2013).
6. M. Wetjen, S. Solchenbach, D. Pritzl, J. Hou, V. Tileli, and H. A. Gasteiger, *Journal of the Electrochemical Society*, **165**, A1503 (2018).
7. R. L. Sacci, J. L. Bañuelos, G. M. Veith, K. C. Littrell, Y. Q. Cheng, C. U. Wildgruber, L. L. Jones, A. J. Ramirez-Cuesta, G. Rother, and N. J. Dudney, *The Journal of Physical Chemistry C*, **119**, 9816 (2015).
8. C. A. Bridges, X.-G. Sun, B. Guo, W. T. Heller, L. He, M. P. Paranthaman, and S. Dai, *ACS Energy Letters*, **2**, 1698 (2017).
9. M. Nagao, C. d. Pitteloud, T. Kamiyama, T. Otomo, K. Itoh, T. Fukunaga, K. Tatsumi, and R. Kanno, *Journal of the Electrochemical Society*, **153**, A914 (2006).
10. S. M. Mamun, M. Herstedt, K. Oikawa, T. Gustafsson, T. Otomo, M. Furusaka, T. Kamiyama, H. Sakaebe, and K. Edstroem, *Applied Physics A: Materials Science & Processing*, **74**, s1028 (2002).
11. S. Seidlmayer, J. Hattendorff, I. Buchberger, L. Karge, H. A. Gasteiger, and R. Gilles, *Journal of the Electrochemical Society*, **162**, A3116 (2015).
12. G. Sandi, K. A. Carrado, R. E. Winans, C. S. Johnson, and R. Csencsits, *Journal of the Electrochemical Society*, **146**, 3644 (1999).
13. G. Sandi, P. Thiyagarajan, K. A. Carrado, and R. E. Winans, *Chem Mater*, **11**, 235 (1999).
14. L. He, S. M. Chathoth, Y. B. Melnichenko, V. Presser, J. McDonough, and Y. Gogotsi, *Microporous and Mesoporous Materials*, **149**, 46 (2012).
15. C. A. Bridges, X.-G. Sun, J. Zhao, M. P. Paranthaman, and S. Dai, *The Journal of Physical Chemistry C*, **116**, 7701 (2012).
16. M. Wetjen, D. Pritzl, R. Jung, S. Solchenbach, R. Ghadimi, and H. A. Gasteiger, *Journal of the Electrochemical Society*, **164**, A2840 (2017).
17. S. Muhlbauer, A. Heinemann, A. Wilhelm, L. Karge, A. Ostermann, I. Defendi, A. Schreyer, W. Petry, and R. Gilles, *Nucl Instrum Meth A*, **832**, 297 (2016).
18. U. Keiderling, *Appl Phys a-Mater*, **74**, S1455 (2002).
19. I. Bressler, J. Kohlbrecher, and A. F. Thunemann, *J Appl Crystallogr*, **48**, 1587 (2015).
20. R. Jung, M. Metzger, D. Haering, S. Solchenbach, C. Marino, N. Tsiouvaras, C. Stinner, and H. A. Gasteiger, *Journal of the Electrochemical Society*, **163**, A1705 (2016).
21. M. Y. Nie, D. P. Abraham, Y. J. Chen, A. Bose, and B. L. Lucht, *J Phys Chem C*, **117**, 13403 (2013).
22. H. Jensen, J. H. Pedersen, J. E. Jorgensen, J. S. Pedersen, K. D. Joensen, S. B. Iversen, and E. G. Sogaard, *J Exp Nanosci*, **1**, 355 (2006).
23. G. M. Veith, M. Doucet, R. L. Sacci, B. Vacaliuc, J. K. Baldwin, and J. F. Browning, *Sci Rep-Uk*, **7** (2017).